IET Electric Power Applications

Research Article

IET Journals
The Institution of Engineering and Technology

Detection of stator incipient faults and identification of faulty phase in three-phase induction motor – simulation and experimental verification

ISSN 1751-8660
Received on 23rd January 2015
Revised on 20th March 2015
Accepted on 17th April 2015
doi: 10.1049/iet-epa.2015.0024
www.ietdl.org

Neerukonda Rama Devi[1] ✉, *Dhanikonda V.S.S. Siva Sarma*[2], *Pulipaka V. Ramana Rao*[3]

[1]*Department of Electrical and Electronics Engineering, Bapatla Engineering College, Bapatla, AP, India*
[2]*Department of Electrical Engineering, NIT Warangal, Warangal, AP, India*
[3]*Department of Electrical and Electronics Engineering, ANU College of Engineering, Guntur, AP, India*
✉ *E-mail: ramadevi_eee@yahoo.co.in*

Abstract: Motor current signature analysis is a well-known method for the diagnosis of stator incipient faults on a three-phase induction motor (IM). In classical motor current signature analysis the fault feature is extracted by analysing the frequency spectrum obtained from the Fourier analysis. However, for proper fault diagnosis, time–frequency domain analysis is required. This study proposes an algorithm based on wavelet analysis for detection of stator incipient faults and identification of faulty phase in three-phase IM. A turn level distributed parameter model of a 3-hp IM is considered for the simulation of inter-turn faults. The parameters used in the simulated model are calculated by conducting experiments on a 3-hp IM. This model is validated by comparing the frequency response of the simulated model with the frequency response measured on practical machine. The proposed algorithm uses an adaptive threshold-based logic for detecting the inter-turn faults and identifying the faulty phase. The algorithm is validated with data generated by the specially designed 3-hp IM. The experimental and simulation results show that the proposed algorithm is effective in detecting the inter-turn faults and identifying the faulty phase even in the presence of supply unbalance conditions.

1 Introduction

AC motors play a major role in modern industrial applications. Squirrel-cage induction motors (IMs) are most frequently used when compared to other motors because of their low cost, ruggedness and low maintenance. One of the key components in IM is the stator winding. According to various motor reliability studies [1, 2], the percentage of motor failures because of stator winding faults are about 37%. Stator winding faults happens mainly because of turn-to-turn, phase-to-phase and winding-to-ground short circuits. The phase-to-phase and phase-to-ground faults start with turn-to-turn short circuit and if undetected leads to major faults. Therefore, early detection of stator inter-turn fault prevents subsequent damage to the motor [3], thereby reducing repair cost and unexpected downtime. It is clear from the literature that non-invasive motor current signature analysis is by far the most preferred technique to diagnose faults [4], because it is more practical and no additional sensors are required. Detection of faults using $dq0$ components [5] and the envelope of the stator currents [6] are just an alternative representation of the same current component. Methods using other signatures, such as slot harmonics [7], pendulous oscillation phenomenon [8] and observer-based method [9] are proposed in the literature. Fault detection using induced voltage at motor terminals when the power supply is turning off is proposed in [10], but this method cannot provide continuous monitoring and protection. There are a number of techniques to detect the stator inter-turn faults using Fourier transform [11, 12]. The Fourier transform is, however, not appropriate to analyse a signal that has a transitory characteristic, such as drifts, abrupt changes and frequency trends. The wavelet techniques can be used for localised analysis in the time–frequency or time-scale domain. Thus, it is a powerful tool for condition monitoring and fault diagnosis [13, 14].

Many proposals have been presented for use of negative sequence component of stator currents that are sensitive to different aspects like stator asymmetry, rotor asymmetry and supply unbalance [15]. The negative-sequence component of current because of motor inherent asymmetry depends on load and slip [16]. An effective diagnostic procedure should distinguish the faulty condition through a negative sequence component of current caused by short circuits apart from the supply unbalance, core saturation, winding asymmetries and eccentricity. Most of the existing techniques require some sort of domain expertise to identify the status of three-phase IM, that is, whether the motor is operating in normal or abnormal condition. Particularly, in signal processing-based techniques the fault detection takes place based on a threshold logic, which is used to distinguish the fault condition from normal condition. Since the fault signature because of the stator inter-turn short circuit is much smaller than the noise level under harsh industrial environment and because of supply unbalance conditions fault detection using fixed threshold is error prone. Hence, an adaptive threshold-based fault detection algorithm is essential for fault diagnosis in a three-phase IM. The stationary wavelet transform (SWT) is suitable for signal noise reduction applications that have been discussed in [17, 18].

This paper proposes an algorithm to detect stator inter-turn fault and identify faulty phase in three-phase IM. The three-phase stator currents are sampled at 6.6 kHz. The three-phase stator currents are analysed with stationary wavelet transform of Biorthogonal 5.5 (Bior5.5) mother wavelet up to sixth level to obtain the three-phase residues. These residues are again decomposed with discrete wavelet transform of same mother wavelet to extract the fault feature. From the extracted fault features, fault index is calculated and compared with adaptive threshold to distinguish the faulty condition from normal condition. The proposed fault detection and phase identification algorithm is tested with data obtained from simulation and experimental setup as well. The severity of the fault is also estimated based on a defined sensitivity

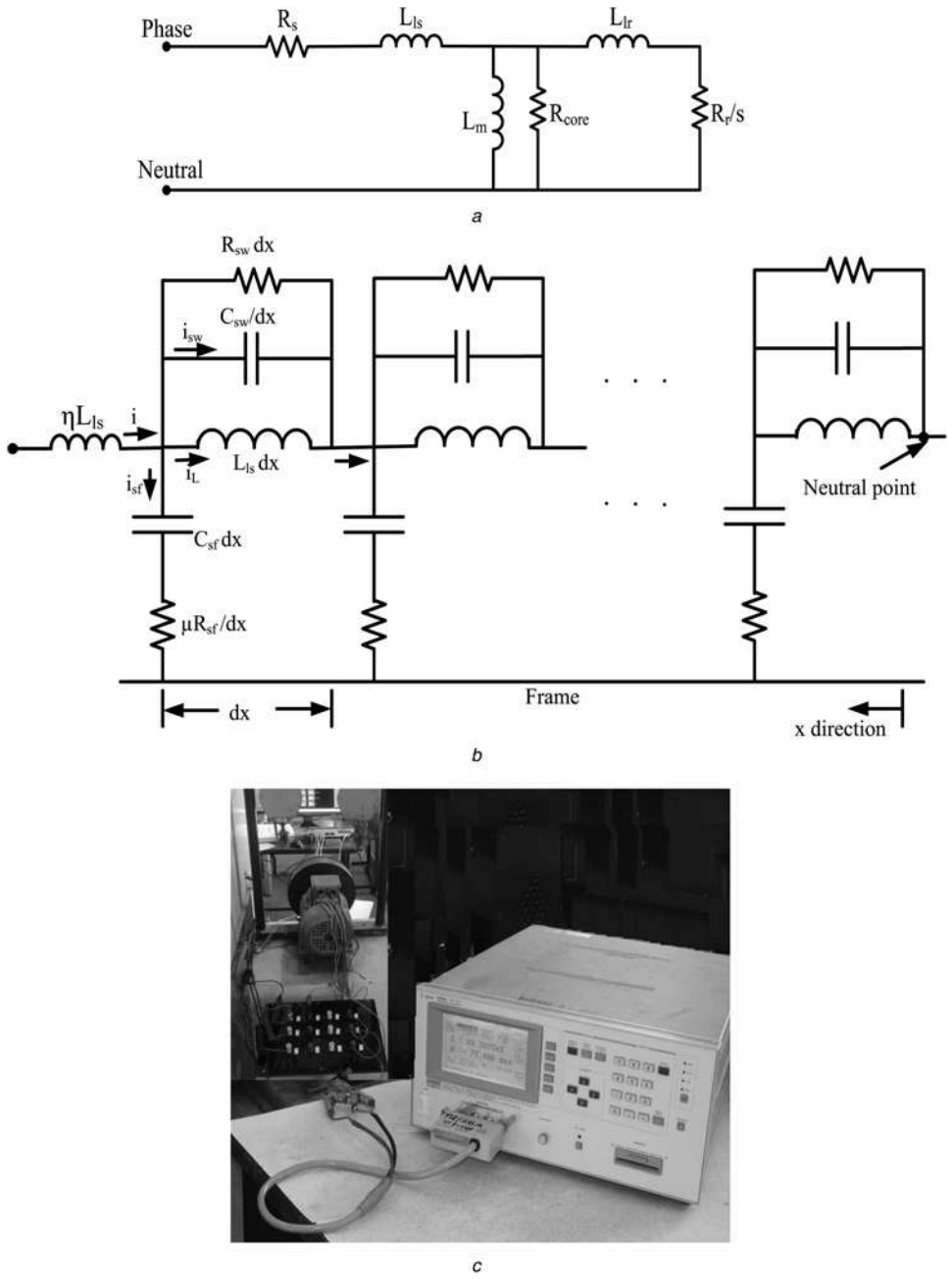

Fig. 1 *Models and experimental setup for three-phase induction motor*

a Low-frequency model for stator winding
b Distributed high frequency model for stator winding
c Experimental setup

index whose value increases with the number of shorted turns. The simulated and experimental results demonstrate the efficacy of the proposed algorithm.

The remaining of this paper is organised as follows: Section 2 describes the distributed parameter model of a three-phase IM and its validation. Brief descriptions of discrete wavelet transform (DWT) and SWT are presented in Section 3. Section 4 gives the description of the proposed fault detection and phase identification algorithm. Finally, the validation of proposed algorithm is presented in Section 5. Conclusions are presented in Section 6.

2 Modelling and simulation

Carrying out numerous experiments on a practical machine to study the behaviour of faults is not practicable as it can lead to the destruction of the machine. However, many parametric studies can be carried out if an accurate and simple model is available to study the behaviour of the motor under stator inter-turn fault condition. In this paper, a low-to-high frequency model is considered to analyse the stator inter-turn faults. Motor behaviour under low frequencies is described by IEEE standard 112 and per phase low-frequency T-equivalent circuit is shown in Fig. 1*a*. In medium to high frequency ranges, a distributed parameter model is best for analysing the motor behaviour. Compared to low-frequency model the distributed parameter model requires extra elements, which are shown in Fig. 1*b*. The additional parameters of the distributed model are calculated from differential mode (DM) and common mode (CM) test which has been discussed in [19].

In general, distributed parameters are determined by measuring the frequency response from DM test setup and CM test setup. A

Table 1 Parameters of a three-phase 3-hp IM

Motor parameters	3-hp IM	Parameters are obtained from
stator resistance (R_s)	9.1 Ω	no load and
stator leakage inductance (L_{ls})	41.38 mH	blocked rotor test
rotor resistance (R_r)	8.08 Ω	
rotor leakage inductance (L_{lr})	31.83 mH	
magnetising Inductance (L_m)	904.44 mH	
core resistance (R_{core})	2842.8 Ω	
stator to frame capacitance (C_{sf})	0.253 nF	DM and CM tests
anti-resonance resistance (μ R_s)	2.667 Ω	
anti-resonance leakage inductance (η L_{ls})	3.547 μH	
stator turn to turn capacitance (C_{sw})	0.853 nF	
stator turn to turn damping resistance (R_{sw})	17 356 Ω	

three-phase, 3-hp, 440 V, 4 pole 50 Hz IM with 36 slots, 6 coils per phase and 72 turns per coil is considered in the present study. The DM test was performed by connecting LCR meter between phase *A* and tied leads of phase *B* and phase *C*. This test procedure is recommended for an ungrounded motor frame and put LCR meter in Z–θ mode. The CM test was performed with ground frame as one probe and phase *A*, phase *B* and phase *C* motor leads tied together to form the second probe to LCR meter in Z–θ mode. Fig. 1*c* shows the experimental setup of a three-phase 3-hp IM. Table 1 presents the low to high frequency parameters of a 3-hp IM.

Figs. 2*a* and *b* show the comparison between measured and simulated frequency responses in DM. These figures demonstrate that the frequency response observed in simulation closely matches with response measured on practical machine. The second resonance impedance wave shape is similar, however, the frequency value in case of simulation is different because of the coil level parameter distribution. Similarly, Figs. 2*c* and *d* illustrate the measured and simulated frequency response in CM. These results show that the measured and simulated response match strongly with each other. Hence the model is valid for transient studies.

3 DWT and SWT

DWT is the most popular wavelet transform, it is widely used in power engineering application, especially in protection systems for the detection, identification, classification and localisation of the power system disturbances both in the time and frequency domains [20]. A threshold is used in wavelet domain to smooth out or to eliminate some coefficients of wavelet transform of the measured signal. The noise content of the signal is reduced effectively under the non-stationary environment, but the results obtained from it were not the optimal mainly because of the loss of the invariant translation property [21]. To overcome this deficiency of DWT, SWT can be used. The SWT is also similar to the DWT in that the low-pass and high-pass filters are applied to the input signal at each level, in which the downsampling stage at each scale is replaced by an upsample of the filter before the convolution. Consider an input signal $x(n)$ of length N where $N=2^J$ for some integer J. Let $g_1(n)$ and $h_1(n)$ be the impulse responses of the low-pass filter and the high-pass filter, respectively. The impulse responses are chosen such that the outputs of the filters are orthogonal to each other. At the first level of SWT, the input signal $x(n)$ is convolved with $g_1(n)$ to obtain the approximation coefficients $a_1(n)$ and with $h_1(n)$ to obtain the detail coefficients $d_1(n)$, that is

$$a_1(n) = g_1(n)^* x(n) = \sum_k g_1(n-k)x(k) \quad (1)$$

$$d_1(n) = h_1(n)^* x(n) = \sum_k h_1(n-k)x(k) \quad (2)$$

In SWT, no sub sampling is performed, $a_1(n)$ and $d_1(n)$ are of length N instead of $N/2$ as in the DWT case. This process is continued recursively. The output of the SWT is then the detail coefficients $d_1(n)$, $d_2(n)$, …, $d_{J0}(n)$ and the approximation coefficients $a_{J0}(n)$ where $J0 < J$. In wavelet de-noising techniques, the threshold selection is very important. Donoho and Johnstone [22] have introduced various threshold schemes and discussed both hard and soft thresholds in a general context. Among these threshold selection rule universal threshold (fixed threshold) selection rule is the most widely used rule. However, in practical application the variance of the noise signal changes time to time. Thus, the threshold should be selected based on an interval or level. Hence a level-based threshold has been selected for the proposed algorithm. The selection of mother wavelet mainly depends on the type of application. In the proposed algorithm, Bior5.5 wavelet has been used as the wavelet basis function for fault detection and phase identification.

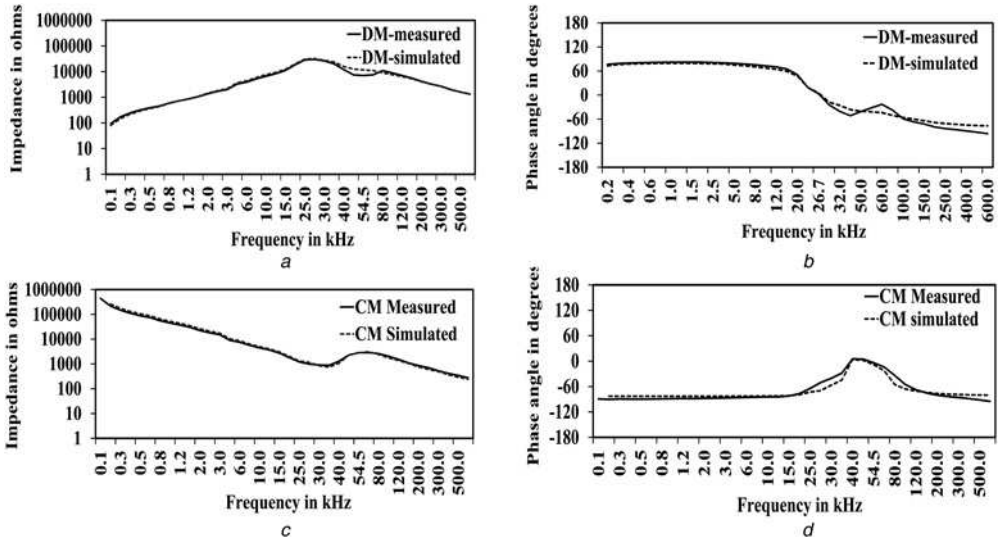

Fig. 2 *Experimental setup and simulation model for creating stator inter-turn faults*

a Impedance against frequency in DM
b Phase angle against frequency in DM
c Impedance against frequency in CM
d Phase angle against frequency in CM

IET Electr. Power Appl., 2015, Vol. 9, Iss. 8, pp. 540–548

4 Fault detection and phase identification algorithm

To detect stator inter-turn faults and identify faulty phase, an efficient fault feature extraction technique is required. In the proposed algorithm, a multi-resolution analysis is used to extract the fault feature. The stator inter-turn fault detection and faulty phase identification algorithm is explained in Algorithm 1 (see Fig. 3). In the proposed algorithm, the level-based threshold reconstruction is used to eliminate the effects because of supply unbalance and machine unbalance. The thresholds for $d1$–$d4$ coefficients are set to a high value for eliminating the high frequency content and the threshold for $d5$ coefficients is set to a high value to eliminate frequency components which are sensitive to supply unbalance. The threshold value of $d6$ coefficients is set to the peak value of $d6$ coefficients during start-up (i.e. healthy condition). The threshold for $d6$ coefficients enhances the fault signature because of the subtraction of healthy coefficients from the captured signal. This process eliminates the effect because of the machine imbalance. The reconstructed signals are called as fault residues. These residues are again decomposed with a DWT of Bior5.5 up to fourth level. The change in residue current because of the fault disturbance is estimated accurately by calculating the ratio between the difference in sample values of the $d1$ coefficients over a moving window of three samples and difference in sample intervals. In discrete signal, the ratio between the difference in sample values and the difference in sample intervals is called as a slope. The slopes of each phase $d1$ coefficients are calculated for identifying the variation levels because of disturbances. A fault is detected by comparing the fault index with adaptive threshold. The fault index I_f and adaptive threshold Th are calculated using the following equations

$$I_f(n) = |\text{slope\_}d1I_R(n)| + |\text{slope\_}d1I_Y(n)| + |\text{slope\_}d1I_B(n)| \quad (3)$$

where $n = 1$: N_1; N_1 is the total number of samples in captured window (1 s); slope_$d1I_R$, slope_$d1I_Y$ and slope_$d1I_B$ are the slopes of $d1$ coefficients of residue currents in R, Y and B phases, respectively

$$\begin{aligned} \text{Th} &= \max(\text{fault index in first cycle}) \\ &\quad \times K \times \max(\text{current in first cycle}) \times \text{factor} \end{aligned} \quad (4)$$

where K is the rise factor and

$$\begin{aligned} \text{factor} &= 2 \text{ if ratio} \le 3 \\ &= \frac{\text{Significand value of } \max(I_f) \text{ in a captured window}}{\text{Largest integer less than the significand value}} \\ &\text{if ratio} > 3 \end{aligned}$$

$$\text{where Ratio} = \frac{\text{Maximum } I_f \text{ in a captured window}}{\text{Maximum } I_f \text{ in 1st cycle}}$$

To identify the faulty phase, calculate the residue energy in each phase based on the slope of the detail coefficients and compare the maximum values of three-phase residue energies over a window of the half cycle from the fault instant. The three-phase residue energies are defined mathematically as follows

$$\text{Energy\_}I_R(n) = \frac{1}{N_2} \sum_{m=n}^{n+N_2-1} [\text{slope\_}d1I_R(m)]^2 \quad (5)$$

$$\text{Energy\_}I_Y(n) = \frac{1}{N_2} \sum_{m=n}^{n+N_2-1} [\text{slope\_}d1I_Y(m)]^2 \quad (6)$$

Algorithm 1

Capture 3-phase stator currents using a data acquisition system.
Decompose 3-phase currents up to 6^{th} level with SWT of Bior5.5 mother wavelet.
Obtain fault residues using reconstructed 3-phase currents.
Obtain $d1$ coefficients by decomposing 3-phase residues with DWT of Bior5.5 mother wavelet.
Calculate the slope of detail coefficients of 3-phase residues and fault index I_f using Eq.(3).
Calculate the adaptive threshold Th using Eq.(4).
Let *count* be the number of fault indices that cross Th over a moving window of 10 samples.
Let t_1 be the instant at which the I_f crosses the Th.
if (*count* for three successive windows < 6) **then**
  Healthy
else
  Let t_2 be the instant from which *count* value is greater than 6 for three successive windows.
  if $((t_1\text{-}t_2) <$ Half cycle) **then**
    Fault is said to occur at location t_2.
    Calculate 3-phase residue energies over a moving window of 6 samples using Eq.(5), Eq.(6) and Eq.(7)
    Find the maximum energy in each phase from fault instant to half cycle.
    if Maximum energy is in R-phase **then**
      Stator inter-turn fault is in R-phase.
    else
      if Maximum energy is in Y-phase **then**
        Stator inter-turn fault is in Y-phase.
      else
        Stator inter-turn fault is in B-phase.
      end if
    end if
  else
    Sudden change in mechanical load.
  end if
end if

Fig. 3 *Proposed fault detection and phase identification algorithm*

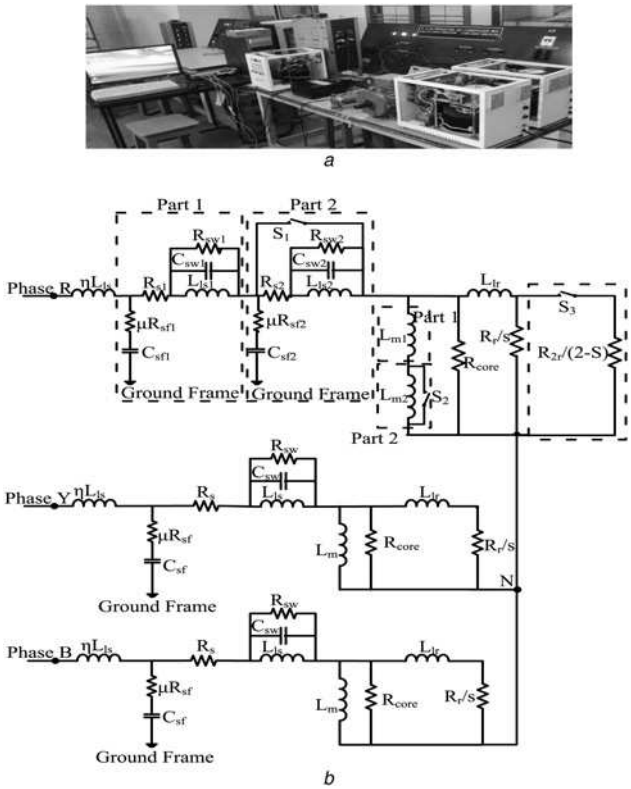

Fig. 4 *Experimental setup for creating stator inter-turn faults*

a Experimental setup for creating stator inter-turn fault in a three-phase 3-hp IM
b Distributed parameter model of a three-phase IM for stator inter-turn fault in R-phase

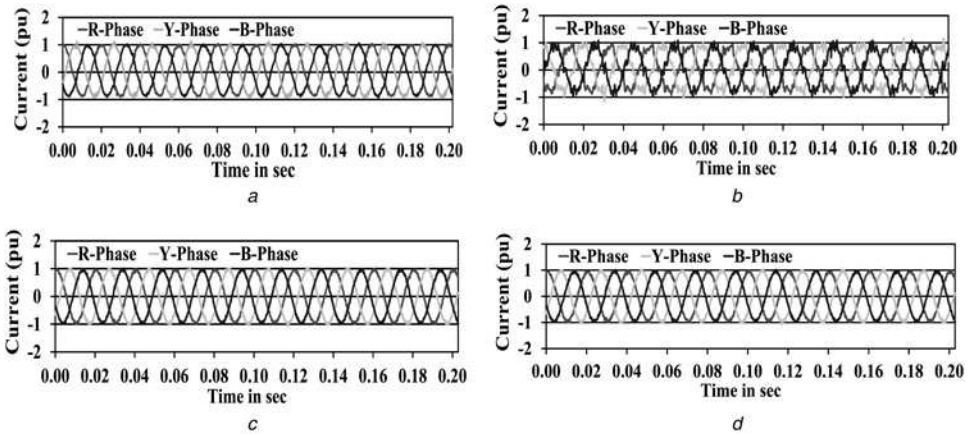

Fig. 5 *Three-phase stator currents of a healthy motor*

Practical cases
a Healthy
b Healthy with 2% supply unbalance
Simulation cases
c Healthy
d Healthy with 2% supply unbalance

$$\text{Energy\_}I_B(n) = \frac{1}{N_2}\sum_{m=n}^{n+N_2-1}[\text{slope\_}d1I_B(m)]^2 \tag{7}$$

where $n = 1$ to N_1–N_2; N_2 = no. of samples in the (1/10)th of the cycle.

5 Testing of the proposed algorithm

An experimental setup was prepared with a three-phase, 3-hp, 4 pole, 50 Hz, 415 V IM with 36 slots, 6 coils per phase and 72 turns per coil. To create the inter-turn short circuit, two tapping points were taken out per phase from the neutral of the stator winding. Each tapping is having a resistance of 0.8 Ω. The inter-turn faults are created experimentally by connecting a suitable resistance between tapping point and ungrounded neural. The three-phase stator currents were captured in 1 s with a sampling frequency of 6.6 kHz by using UNIPOWER DIP 8000 network analyser. To acquire the signals the network analyser is connected to a personal computer. Fig. 4*a* shows the experimental setup for creating stator inter-turn faults.

To simulate the stator inter-turn faults a three-phase, 3-hp, 415 V, 50 Hz IM with a star-connected stator winding is considered. The stator winding corresponding to the phase in which the fault is created is divided into two parts. An additional branch is connected in parallel to the rotor resistance to simulate the disturbance component because of the stator inter-turn fault. The fault is created by closing three switches as shown in Fig. 4*b* and it illustrates the stator inter-turn fault in *R*-phase of a three-phase IM. In this figure, Part 1 refers to a healthy portion of the winding and Part 2 refers the shortened turns of the winding. The resistance, inductance and insulation capacitance are divided into proportion to the number of short circuited turns. The various percentages of turn-level short circuits in different phases have been simulated in the MATLAB/Simulink environment. To bring the simulation model more closer to practical scenarios Gaussian noise is injecting in each phase. The noise level to be injected is calculated from the captured three-phase stator currents in the experimental setup.

5.1 Detection of fault

Four conditions were considered for validating the algorithm, such as healthy, healthy with supply unbalance, inter-turn fault and inter-turn fault with supply unbalance. The sensitivity of the fault

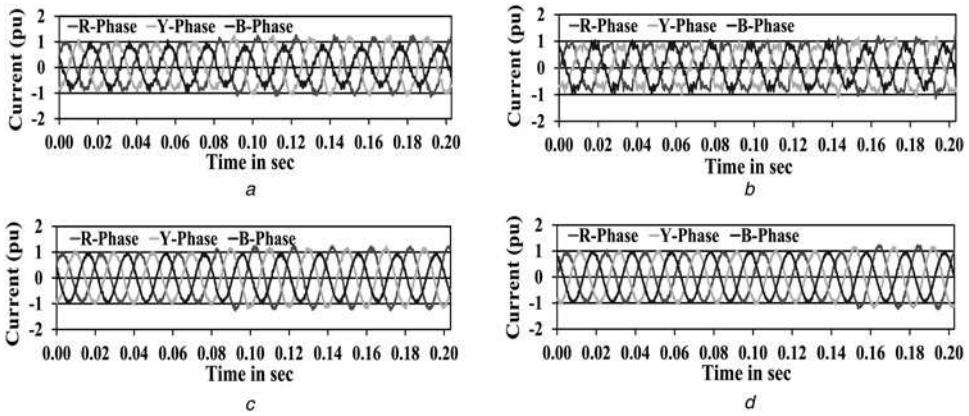

Fig. 6 *Three-phase stator currents of a motor with fault in R-phase*

Practical cases
a 8-turn shorted fault
b 8-turn shorted fault with 2% supply unbalance
Simulation cases
c 8-turn shorted fault
d 8-turn shorted fault with 2% supply unbalance

IET Electr. Power Appl., 2015, Vol. 9, Iss. 8, pp. 540–548

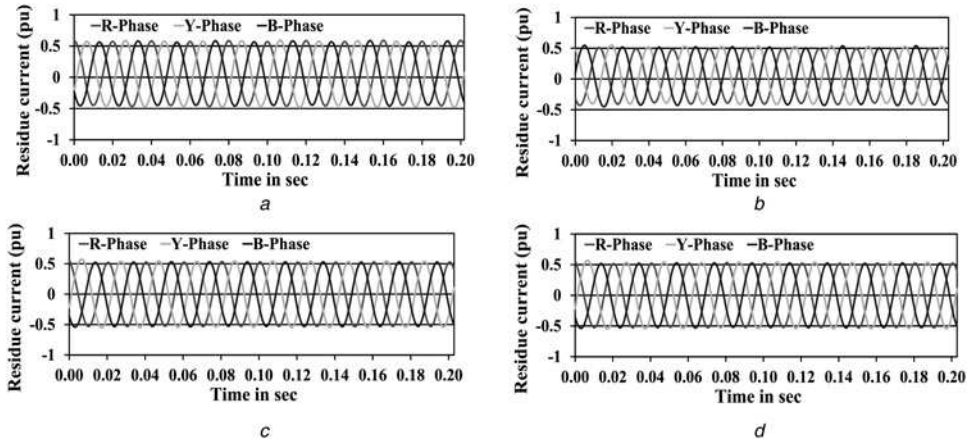

Fig. 7 *Three-phase residue currents of healthy motor*

Practical cases
a Healthy
b Healthy with 2% supply unbalance
Simulation cases
c Healthy
d Healthy with 2% supply unbalance

with four levels of short circuited turns via 2-turn, 4-turn, 6-turn and 8-turn short circuit per phase is analysed. Three-phase stator currents for healthy cases of practical and simulation are shown in Fig. 5. The 8-turn shorted fault cases of practical and simulation are illustrated in Fig. 6. The three-phase residues for healthy cases of practical and simulation studies are illustrated in Fig. 7. Similarly, Fig. 8 represents the three-phase residues for 8-turn shorted fault cases of practical and simulation.

To extract the fault feature and its occurrence, again decompose the three-phase residues up to fourth level by using DWT of Bior5.5 mother wavelet and calculate the slopes of the detail coefficients. Fault index I_f and adaptive threshold Th are calculated by using (3) and (4), respectively. A fault is detected when the difference between the time instants t_2 and t_1 is less than a half cycle. Figs. 9*a* and *b* demonstrate the fault indices I_f along with adaptive threshold Th in the healthy and fault condition of a three-phase IM for practical cases of healthy with balanced supply and 8-turn shorted fault with 2% supply unbalance, respectively. Similarly, Figs. 9*c* and *d* represent the simulation cases of healthy with balanced supply and 8-turn shorted fault with 2% supply unbalance, respectively. Figures for healthy cases show that the fault indices I_f are less than the Th. However, in case of faults the fault indices I_f cross the Th from the fault instant. Thus the difference between the time interval of t_2 and t_1 is always less than a half cycle. The fault is detected effectively even the supply unbalance is changed to 3%. In simulation, the fault detection algorithm is also tested with various levels of supply unbalances ranging from 1 to 5%, but the fault detection algorithm is not susceptible to supply unbalance conditions. Hence the stator inter-turn fault detection algorithm is effective in detecting the stator incipient faults in presence of supply unbalance.

To validate the proposed algorithm, a comparison is made between the relative value of maximum fault index (RMFI) and relative value of adaptive threshold (RAT) for various fault cases of practical and simulated studies. The RMFI and RAT are mathematically expressed using (8) and (9), respectively. Table 2 depicts the correctness of the proposed algorithm for various cases of practical and simulation studies. From this table, even for small fault, that is, 2-turn shorted fault the RMFI of practical case is in good agreement with that of simulation case. The difference in the

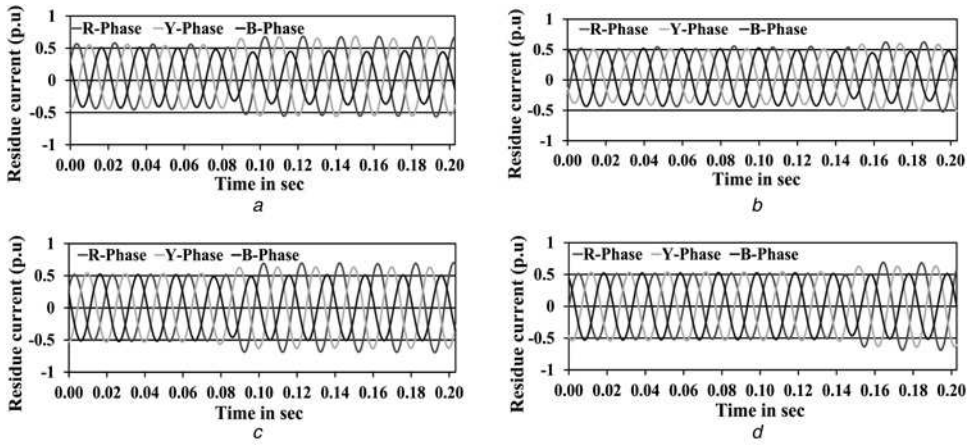

Fig. 8 *Three-phase residue currents of a motor with fault in R-phase*

Practical cases
a 8-turn shorted fault
b 8-turn shorted fault with 2% supply unbalance
Simulation cases
c 8-turn shorted fault
d 8-turn shorted fault with 2% supply unbalance

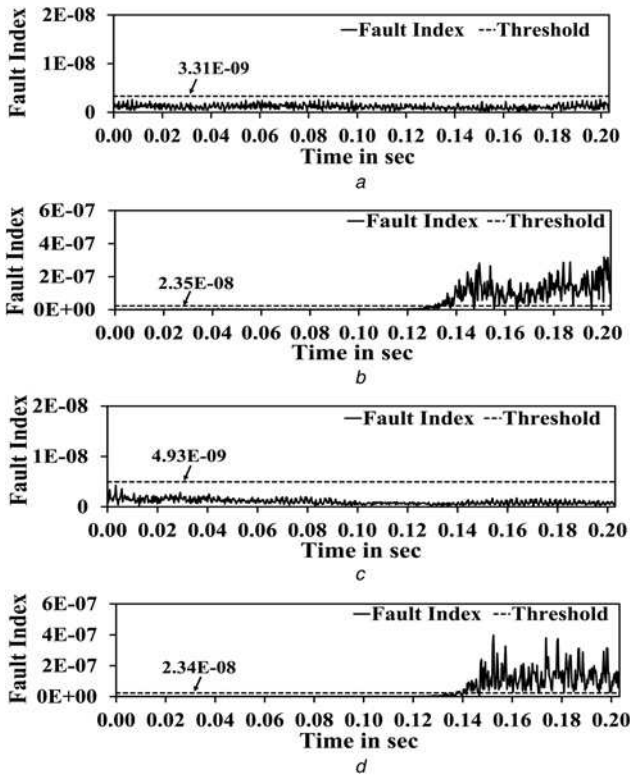

Fig. 9 *Variation in fault indices*

Practical
a Healthy
b 8-turn fault with 2% supply unbalance
Simulation
c Healthy
d 8-turn fault with 2% supply unbalance

values for the practical and simulation case is mainly because of the reason that the noise variance is kept constant in the simulation, which is not true in actual practice

$$\text{RMFI} = \frac{\text{Maximum value of } I_f \text{ under fault condition}}{\text{Maximum value of } I_f \text{ under healthy condition}} \quad (8)$$

$$\text{RAT} = \frac{\text{Th under fault condition}}{\text{Th under healthy condition}} \quad (9)$$

To study the effect of variation in stator temperature on the proposed fault detection algorithm a simulation study is carried out by changing the effective stator resistance corresponding to the changes in temperature of the stator starting from 26 to 46°C in 2° increments for an 8-turn shorted fault. Table 3 shows the relative variation in the maximum value of fault index and adaptive threshold values with respect to their corresponding values when

Table 2 Comparison of fault detection criteria for various practical and simulation cases with respect to healthy conditions

Cases	Practical		Simulation	
	RMFI	RAT	RMFI	RAT
2-turn fault	34.33	1.35	23.20	1.17
2-turn fault with 2% supply unbalance	19.59	0.84	10.33	0.72
4-turn fault	78.50	4.66	66.30	3.28
4-turn fault with 2% supply unbalance	69.67	3.18	61.09	3.68
6-turn fault	133.82	4.31	124.39	3.45
6-turn fault with 2% supply unbalance	121.13	7.59	114.86	4.12
8-turn fault	159.62	3.25	145.87	3.52
8-turn fault with 2% supply unbalance	170.34	4.11	127.25	4.11

Table 3 Temperature effects on maximum value of fault index and adaptive threshold for an 8-turn short circuit

Percentage of temperature rise w.r.t. 26°C, %	Relative variation in maximum value of I_f, %	Relative variation in adaptive threshold, %
7.69	−0.34	0.08
15.38	−0.68	−0.25
23.08	−1.03	−0.58
30.77	−1.37	−0.90
38.46	−1.69	−1.21
46.15	−2.05	−1.55
53.85	−2.39	−1.88
61.54	−2.73	−2.20
69.23	−3.07	−2.52
76.92	−3.41	−2.85

the stator is at the room temperature. It is apparent from Table 3 that the variation in stator temperature has very little effect on the key parameters of the fault detection algorithm namely adaptive threshold and maximum value of fault index. Hence the performance of the proposed fault detection algorithm is not susceptible to variations in stator temperature.

5.2 Identification of faulty phase

The faulty phase is identified by comparing the maximum value of residue energy in three-phases over a window size of the half cycle from the fault instant. The variations in three-phase residue energies for practical cases of 8-turn shorted fault and 8-turn fault with 2% supply unbalance are illustrated in Figs. 10*a* and *c*, respectively. Similarly, for simulation cases the variation in energy residues are shown in Figs. 10*b* and *d*. From the figures, the

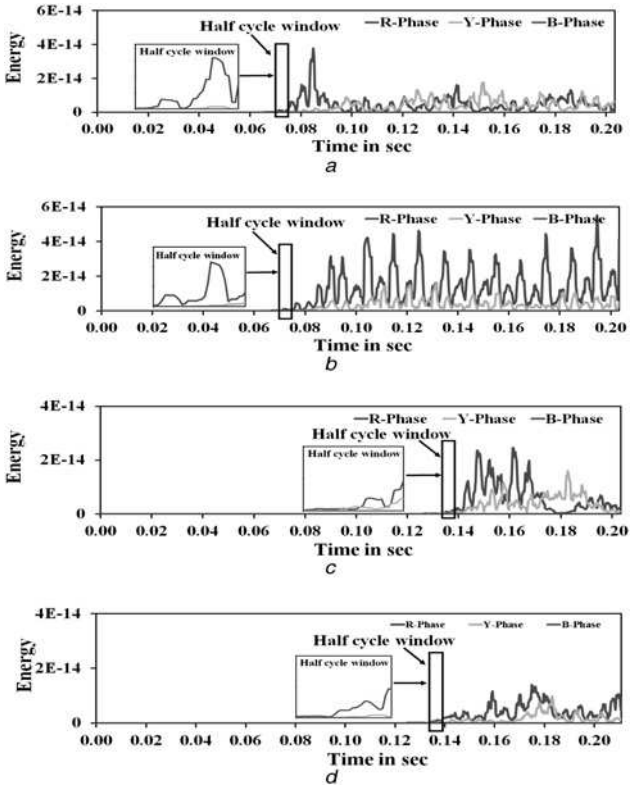

Fig. 10 *Three-phase residue energies of R-fault cases*

Practical
a 8-turn short circuit
c 8-turn short circuit with 2% supply unbalance
Simulation
b 8-turn short circuit
d 8-turn short circuit with 2% supply unbalance

magnified window of the half cycle clearly shows that the residue energy in the faulty phase is higher than that of other phases. Hence the proposed algorithm identifies the faulty phase accurately even in the presence of supply unbalance.

5.3 Severity of inter-turn fault

The severity of the stator inter-turn fault can be identified based on the sensitivity index, which is defined as the ratio of post-fault and pre-fault mean energies of the fourth level approximate coefficients of the three-phase residues in a captured window of 1 s duration. Two tests were performed keeping the load constant, while changing the number of shortened turns. Figs. 11*a–c* illustrate the sensitivity index of practical and simulation cases with and without supply unbalance in *R*-phase, *Y*-phase and *B*-phase shorted faults, respectively. From the results, it can be concluded that the sensitivity indices in practical case without supply unbalance is closer to the practical case with supply unbalance and simulation cases also in the whole range of faults. Thus the severity of the fault is not sensitive to supply unbalances. It is observed that, the sensitivity index grows as the number of shortened turns increases.

Figs. 12*a–c* illustrate the sensitivity index of 10-hp motor for *R*-phase, *Y*-phase and *B*-phase, respectively. The variation in sensitivity index with the increase in the level of shortened turns is more in 10-hp motor when compared with a 3-hp IM. It is mainly because of the higher value of potential difference between adjacent turns. Thus the level of short-circuited turns is identified more prominently in higher rated motors by using the sensitivity index.

The total number of coils per phase and turns per coil for a 3-hp IM are 6 and 72, respectively, and for a 10-hp IM 4 and 54, respectively. For a given supply voltage, the voltage across turn–turn of a 10-hp motor is more than that of a 3-hp motor. Hence the sensitivity index of a 10-hp motor is more than that of a 3-hp motor, for a given level of short-circuited turns which is obvious from the experimental results in the case of *R*-phase fault as shown in Fig. 12*d* and the same trend is observed in both *Y*-phase and *B*-phase fault cases.

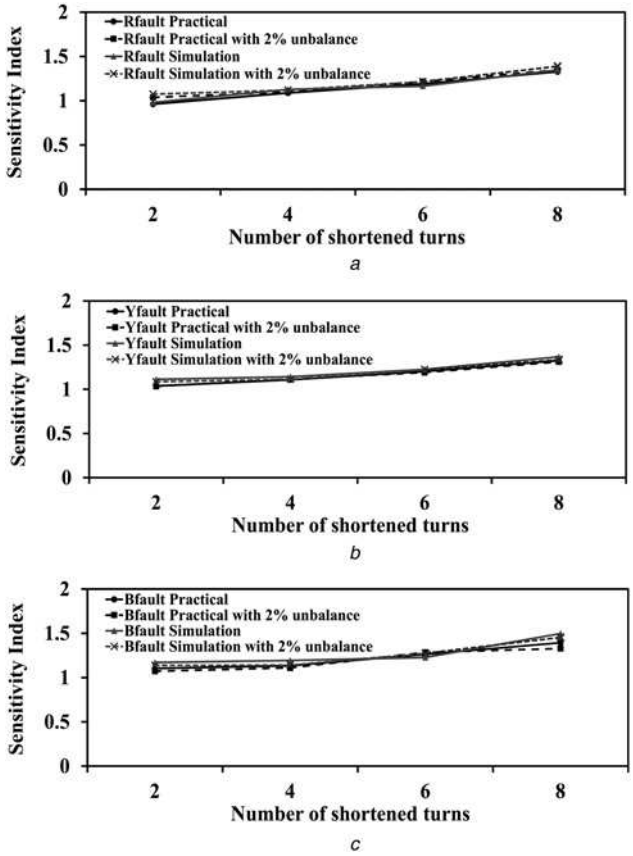

Fig. 11 *Variation in sensitivity index of stator inter-turn faults for a 3-hp motor*

a *R*-phase
b *Y*-phase
c *B*-phase

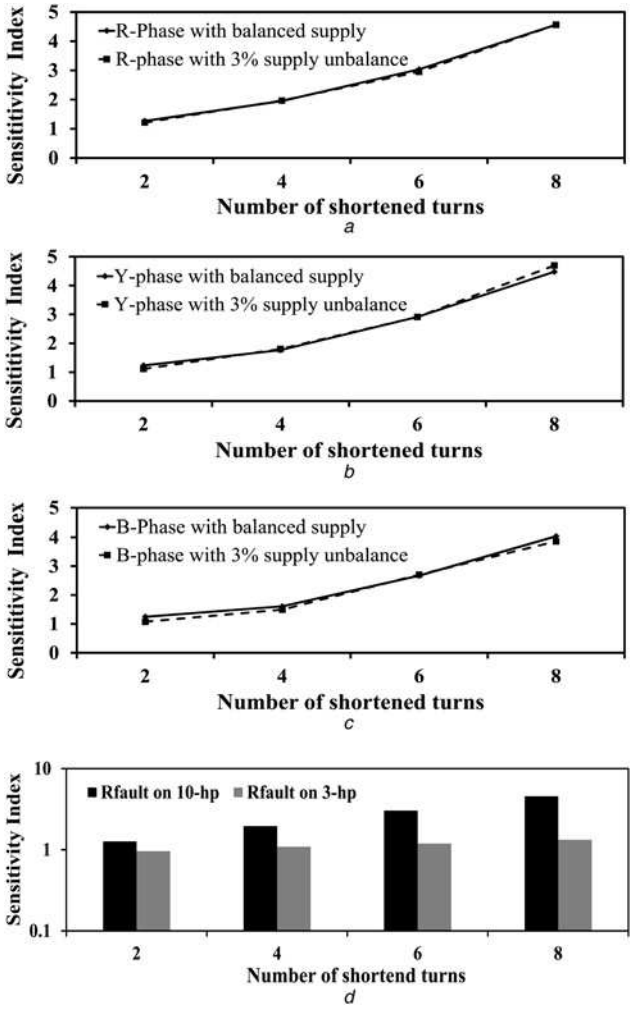

Fig. 12 *Variation in sensitivity index of stator inter-turn faults for a 10-hp motor*

a *R*-phase
b *Y*-phase
c *B*-phase
d *R*-phase fault compared with that of a 3-hp motor

6 Conclusions

This paper proposes an algorithm, to detect the stator inter-turn fault and identify the faulty phase by using wavelet-based multi resolution analysis. The detection algorithm is a combination of the SWT and DWT. The outcome of the proposed algorithm is not affected by supply unbalance conditions of the machine. The fault signature is extracted effectively by using SWT instead of DWT because of shift invariance property of SWT. Fault residue currents are obtained from the inverse stationary wavelet transform of Bior5.5 mother wavelet and again decomposed with a DWT of the same mother wavelet. The fault indices and energies of the three-phases are obtained from the slope of detail level coefficients of three-phase fault residue and compared with adaptive threshold to detect the fault and identify the faulty phase. The proposed algorithm gives better performance to detect the stator inter-turn

fault and identify the faulty phase because of the adaptive threshold. The effectiveness of the proposed fault detection and phase identification algorithm is demonstrated with simulation and experimental results. The variation in sensitivity index with the increase in the number of shortened turns for a 3-hp motor is small when compared with the variation in sensitivity index for a 10-hp motor. This is because of the small potential difference between adjacent turns in case of 3-hp motor. The sensitivity index of the fault also identifies the level of shorted turns even in the presence of supply unbalance conditions.

7 References

1 Bell, R., McWilliams, D., O'donnell, P., Singh, C., Wells, S.: 'Report of large motor reliability survey of industrial and commercial installations. I', *IEEE Trans. Ind. Appl.*, 1985, **21**, (4), pp. 853–864

2 Bell, R., Heising, C., O'donnell, P., Singh, C., Wells, S.: 'Report of large motor reliability survey of industrial and commercial installations. ii', *IEEE Trans. Ind. Appl.*, 1985, **21**, (4), pp. 865–872

3 Siddique, A., Yadava, G., Singh, B.: 'A review of stator fault monitoring techniques of induction motors', *IEEE Trans. Energy convers.*, 2005, **20**, (1), pp. 106–114

4 El Hachemi Benbouzid, M.: 'A review of induction motors signature analysis as a medium for faults detection', *IEEE Trans. Ind. Electron.*, 2000, **47**, (5), pp. 984–993

5 Cruz, S.M., Cardoso, A.M.: 'Stator winding fault diagnosis in three-phase synchronous and asynchronous motors, by the extended park's vector approach', *IEEE Trans. Ind. Appl.*, 2001, **37**, (5), pp. 1227–1233

6 Da Silva, A.M., Povinelli, R.J., Demerdash, N.A.: 'Induction machine broken bar and stator short-circuit fault diagnostics based on three-phase stator current envelopes', *IEEE Trans. Ind. Electron.*, 2008, **55**, (3), pp. 1310–1318

7 Joksimovic, G.M., Penman, J.: 'The detection of inter-turn short circuits in the stator windings of operating motors', *IEEE Trans. Ind. Electron.*, 2000, **47**, (5), pp. 1078–1084

8 Mirafzal, B., Povinelli, R.J., Demerdash, N.A.: 'Interturn fault diagnosis in induction motors using the pendulous oscillation phenomenon', *IEEE Trans. Energy Convers.*, 2006, **21**, (4), pp. 871–882

9 De Angelo, C.H., Bossio, G.R., Giaccone, S.J., Valla, M.I., Solsona, J.A., García, G.O.: 'Online model-based stator-fault detection and identification in induction motors', *IEEE Trans. Ind. Electron.*, 2009, **56**, (11), pp. 4671–4680

10 Nandi, S., Toliyat, H.A.: 'Novel frequency-domain-based technique to detect stator interturn faults in induction machines using stator- induced voltages after switch-off', *IEEE Trans. Ind. Appl.*, 2002, **38**, (1), pp. 101–109

11 Nandi, S., Toliyat, H.A., Li, X.: 'Condition monitoring and fault diagnosis of electrical motors-a review', *IEEE Trans. Energy Convers.*, 2005, **20**, (4), pp. 719–729

12 Sharifi, R., Ebrahimi, M.: 'Detection of stator winding faults in induction motors using three-phase current monitoring', *ISA Trans.*, 2011, **50**, (1), pp. 14–20

13 Khan, M., Radwan, T.S., Rahman, M.A.: 'Real-time implementation of wavelet packet transform-based diagnosis and protection of three-phase induction motors', *IEEE Trans. Energy Convers.*, 2007, **22**, (3), pp. 647–655

14 Das, S., Purkait, P., Dey, D., Chakravorti, S.: 'Monitoring of inter-turn insulation failure in induction motor using advanced signal and data processing tools', *IEEE Trans. Dielectrics Electr. Insul.*, 2011, **18**, (5), pp. 1599–1608

15 Zhang, P., Du, Y., Habetler, T.G., Lu, B.: 'A survey of condition monitoring and protection methods for medium-voltage induction motors', *IEEE Trans. Ind. Appl.*, 2011, **47**, (1), pp. 34–46

16 Kliman, R.A.K.G.B., Premerlani, W.J., Hoeweler, D.: 'A new approach to on-line turn fault detection in ac motors'. Conf. Rec. 31st, IEEE IAS Annual Meeting, 1996, vol. 1, pp. 687–693

17 Hernández, O., Olvera, E.: 'Noise cancellation on ecg and heart rate signals using the undecimated wavelet transform'. IEEE Int. Conf. on eHealth, Telemedicine, and Social Medicine, 2009, eTELEMED'09, 2009, pp. 145–150

18 Akshay, N., Jonnabhotla, N.A.V., Sadam, N., Yeddanapudi, N.D.: 'Ecg noise removal and qrs complex detection using uwt'. IEEE Int. Conf. on Electronics and Information Engineering (ICEIE), 2010, 2010, vol. 2, pp. V2–438

19 Mirafzal, B., Skibinski, G., Tallam, R., Schlegel, D., Lukaszewski, R.: 'Universal induction motor model with low-to-high frequency-response characteristics', *IEEE Trans. Ind. Appl.*, 2007, **43**, (5), pp. 1233–1246

20 Youssef, O.A.: 'Online applications of wavelet transforms to power system relaying', *IEEE Trans. Power Deliv.*, 2003, **18**, (4), pp. 1158–1165

21 Darwish, H.A., Hesham, M., Taalab, A.-M., Mansour, N.M.: 'Close accord on dwt performance and real-time implementation for protection applications', *IEEE Trans. Power Deliv.*, 2010, **25**, (4), pp. 2174–2183

22 Donoho, D.L., Johnstone, I.M.: 'Threshold selection for wavelet shrinkage of noisy data'. IEEE Int. Conf. on Engineering Advances: New Opportunities for Biomedical Engineers 1994, 1994, pp. A24–A25